Volume 9 | Number 16 | 21 August 2019 | Pages 4151–4454

Catalysis Science & Technology

rsc.li/catalysis

ISSN 2044-4761

ROYAL SOCIETY OF CHEMISTRY | Celebrating IYPT 2019

PAPER
Nikolay Kosinov, Emiel J. M. Hensen *et al.*
Mild dealumination of template-stabilized zeolites by NH_4F

Catalysis Science & Technology

PAPER

View Article Online
View Journal | View Issue

Cite this: *Catal. Sci. Technol.*, 2019, **9**, 4239

Mild dealumination of template-stabilized zeolites by NH_4F†

Aleksei Bolshakov, Nikolay Kosinov,* Douglas E. Romero Hidalgo, Brahim Mezari, Arno J. F. van Hoof and Emiel J. M. Hensen*

Received 27th March 2019,
Accepted 10th June 2019

DOI: 10.1039/c9cy00593e

rsc.li/catalysis

A novel method to remove aluminium from the framework of as-synthesized zeolite crystals is presented. Hydrothermal treatment in an aqueous ammonium fluoride solution leads to selective dealumination of ZSM-5–TPA zeolite crystals. The optimized dealumination procedure results in 30–50% removal of Al atoms without significant structural degradation. It is also shown that template stabilization by tetrapropylammonium cations or pentaerythritol plays a key role in the developed method, as template-free ZSM-5 crystals, treated under similar conditions, lose their crystallinity and microporosity. The mild dealumination was applied to as-synthesized hierarchical mordenite zeolite to obtain a much more effective catalyst in hydroconversion of heavy paraffins. The optimized Pd/MOR catalyst showed a low selectivity to cracked products up to 60% of *n*-hexadecane conversion with product distribution close to the ideal hydrocracking regime.

1. Introduction

Fluorine is widely used in the synthesis and chemical modification of zeolites.[1] Remarkable progress in the field of zeolite synthesis has been achieved, since the fluoride route method was reported in the 1970s.[2] New zeolite topologies,[3,4] large zeolite crystals[5,6] and various zeotype materials[7–9] could be synthesized under near-neutral pH conditions. A particular influence of the fluoride route is the significant reduction of the amount of silanol defects, resulting in more hydrophobic and hydrothermally stable materials in comparison to zeolites conventionally prepared in alkaline media.[10–12] More recently, it has also been reported that introduction of NaF during the synthesis of high-silica CHA zeolites results in additional (intracrystalline) microporosity, which can greatly enhance mass transport of reactants to active sites during catalysis.[13,14] Framework etching with HF or NH_4HF_2 is another method to introduce additional porosity in zeolites.[15–18] Furthermore, substitution of surface hydroxyls with fluoride groups involving for instance organosilane grafting can be employed to enhance the surface hydrophobicity.[19,20] Recently, Tuel and coworkers showed that it is also possible to "exchange" silanol defects (SiO^-) in as-synthesized siliceous zeolites by F anions. This method heals defects in the zeolite framework. The reverse exchange of the fluoride form back to a defect form one by a hydrothermal treatment with NH_4OH has also been described.[21]

Fluoride compounds can also be used to dealuminate zeolites. Post-synthesis dealumination of zeolites is a versatile strategy to obtain model zeolite materials with particular physio-chemical properties. For instance, extraction of aluminum from low-silica zeolites is often necessary to increase the intrinsic Brønsted acidity of the zeolites and improve their (hydro)thermal stability without destroying the framework.[22–24] The conventional method to dealuminate zeolite by steam calcination and acid leaching causes a significant number of lattice defects in the form of silanol nests and additional mesoporosity.[25,26] Another approach is to substitute zeolite framework aluminum for silicon using *e.g.* ammonium hexafluorosilicate $(NH_4)_2SiF_6$, which allows nearly defect-free zeolites with a lower aluminum content to be obtained.[27] This method has a limited applicability due to the toxicity and cost of the $(NH_4)_2SiF_6$ reagent. Additionally, the big size of the SiF_6^{2-} ion makes this approach only amenable to a limited number of zeolite topologies containing 12-membered ring pores.[28,29]

In this work we demonstrate how hydrothermal treatment of as-synthesized TPA–ZSM-5 crystals (TPA = tetrapropylammonium) using an aqueous solution of NH_4F under autogenous pressure can result in the selective replacement of framework aluminum by silicon. We employ ^{27}Al and ^{29}Si MAS NMR spectroscopy, XRD, Ar physisorption, electron microscopy, XPS and ICP to characterize the samples before

Laboratory of Inorganic Materials and Catalysis, Schuit Institute of Catalysis, Department of Chemical Engineering and Chemistry, Eindhoven University of Technology, P.O. Box 513, 5600 MB Eindhoven, The Netherlands.
E-mail: n.a.kosinov@tue.nl, e.j.m.hensen@tue.nl

† Electronic supplementary information (ESI) available: Additional NMR spectra, Ar adsorption and FTIR results, XRD patterns and SEM images. See DOI: 10.1039/c9cy00593e

and after treatment. We optimize the treatment time, temperature and NH_4F concentration. Under optimized conditions, this approach can lower the amount of defects and increase the crystallinity of zeolites. We also show that the presence of charged or neutral template molecules inside the micropores is a prerequisite for this method.

2. Experimental

2.1 Synthesis of materials

ZSM-5–TPA zeolite was synthesized as follows. Sodium hydroxide (Sigma Aldrich, 99%), tetrapropylammonium hydroxide (TPAOH, Merck, 40 wt%), sodium aluminate (Sigma Aldrich, technical) were mixed with deionized water and stirred for 20 min at room temperature. Subsequently, colloidal silica Ludox AS-40 (Sigma Aldrich, 40 wt%) was added quickly into the formed solution. The final synthesis gel had a molar composition of 3 TPAOH : 0.7 Na_2O : 0.5 Al_2O_3 : 20 SiO_2 : 1500 H_2O. After vigorous stirring at 25 °C for 5 h, the resulting gel was transferred into a PTFE-lined stainless steel autoclave and crystallized at 160 °C for 120 h while tumbling at 60 rpm.

For the synthesis of ZSM-5–PET, sodium hydroxide (Sigma Aldrich, 99%) and pentaerythritol (PET, Sigma Aldrich, 99%) were used. Sodium aluminate, sodium hydroxide and pentaerythritol were mixed with deionized water in a PTFE beaker and stirred for 20 min. Afterwards, Ludox AS-40 was added quickly into the clear solution. The final gel had a molar composition of 6.7 PET : 3.25 Na_2O : 0.5 Al_2O_3 : 20 SiO_2 : 976 H_2O. After vigorous stirring at room temperature for 2 h, the resulting gel was transferred into a PTFE-lined stainless-steel autoclave and crystallized at 175 °C for 48 h while tumbling at 60 rpm.

2.2 Treatment with NH_4F

Fluoride treatment of the resulting zeolites was carried out in aqueous NH_4F (Sigma Aldrich, 98%) solution using the following typical procedure. An amount of 0.55 g of as-synthesized ZSM-5 zeolite was dispersed in 38 ml of 1 M NH_4F solution and reacted at 175 °C for 6 h into a PTFE-lined stainless-steel autoclave while tumbling at 60 rpm. The NH_4F concentration was varied in the 0.2–5 M range, and the temperature and the treatment time were varied between 165–195 °C and 2–168 h, respectively. The treated products were thoroughly washed with hot (~90 °C) deionized water and dried in air at 110 °C overnight. Finally, the samples were calcined at 550 °C for 5 h in air. The protonated form of the zeolites was obtained by three subsequent steps of ion-exchange of the as-synthesized samples with 1.0 M NH_4NO_3 solution (1 g of the solid per 100 mL) for 3 hours at 70 °C. The zeolites in the NH_4 form were dried overnight at 110 °C and calcined at 550 °C for 5 h to acquire the acidic form of the zeolites.

2.3 Preparation of the Pd/MOR catalyst

The samples in the proton form were loaded with 1 wt% Pd by incipient wetness impregnation with an aqueous $Pd(NH_3)_4(NO_3)_2$ solution. The resulting catalysts were calcined at 450 °C under flowing air for 4 h.

2.4 Characterization

Thermogravimetric analysis (TGA). TG analyses of the zeolite samples were performed on a Mettler Toledo TGA/DSC 1 instrument. About 10 mg of a catalyst sample was placed in an alumina crucible. The uncovered crucible was heated up to 750 °C at a rate of 10 °C min^{-1} in 40 mL min^{-1} He and 20 mL min^{-1} O_2 flow.

X-ray photoelectron spectroscopy (XPS). The surface of the materials was probed by XPS using a Thermo Scientific K-alpha spectrometer equipped with a monochromatic Al Kα X-ray source (1486.6 eV) with a 180° double-focusing hemispherical analyzer including a 128-channel detector. A spot size in all measurements was set to 400 μm. High resolution spectra of C 1s, Si 2p and Al 2p regions were recorded with a pass energy of 50 eV, while survey spectra were recorded with a pass energy of 200 eV. XPS depth profiling (DP-XPS) was done by high-energy Ar^+ sputtering ($p = 1 \times 10^{-7}$ mbar, 2 kV) with time steps of 20 s. XPS spectra were taken after each sputtering step. Based on the depth profiles, the Si/Al ratios were determined as a function of the depth. The obtained spectra were analyzed by using CasaXPS software. When quantifying the XPS spectra, relative sensitivity factors (RSF) were used to transform the measured peak areas of the Si 2p (RSF 0.817) and Al 2p (RSF 0.537) signals into percentage atomic concentration. In this case, the Si/Al molar ratio can be calculated as a relationship between Si and Al atomic concentrations.

Ar physisorption. Textural properties were analyzed by Ar physisorption, which was carried out at −186 °C using a Micromeritics ASAP-2020 apparatus. The samples were outgassed at 400 °C in a dynamic vacuum ($p < 5$ μbar) overnight prior to the measurements. The microporous volume was determined by the *t*-plot method in a thickness range from 4.0 Å to 6.0 Å.

ICP-OES. The elemental composition of the zeolites was determined by ICP-OES (inductively coupled plasma optical emission spectroscopy) using a Spectro CIROS CCD ICP spectrometer with axial plasma viewing. Prior to analysis, the samples were dissolved in a 1 : 1 : 1 (by weight) mixture of HF (40%) : HNO_3 (60%) : H_2O.

IR spectroscopy. Transmission IR spectra of the zeolites were recorded on a Bruker Vertex 70v spectrometer in the range of 4000–400 cm^{-1}. Spectra were acquired at 2 cm^{-1} resolution and 64 scans. The samples were prepared as thin wafers of ~12 mg and placed inside a controlled environment infrared transmission cell. After calcination at 550 °C in an air flow the sample was cooled down till 150 °C and measured in a dynamic vacuum.

X-ray diffraction (XRD). XRD patterns were recorded using a Bruker D_2 Endeavor powder diffraction system. Cu Kα radiation in the 2θ range of 5–60° with a step size of 0.02° and a time step of 0.4 s.

Transmission electron microscopy (TEM). Transmission electron microscopy (TEM) pictures were taken on an FEI Tecnai 20 at 200 kV. The samples were suspended in ethanol and dispersed over a carbon coated holey Cu grid with a film prior to measurements.

Scanning electron microscopy (SEM). SEM images were taken using an FEI Quanta 200F scanning electron microscope at an accelerating voltage of 3 kV and a spot size of 4.5.

NMR spectroscopy. Nuclear magnetic resonance (NMR) spectra were measured using an 11.7 Tesla Bruker DMX500 NMR spectrometer operating at 500 MHz, 470 MHz, 99 MHz and 132 MHz for ^{1}H, ^{19}F, ^{29}Si and ^{27}Al, respectively. ^{27}Al and ^{19}F MAS NMR spectra were recorded using a Bruker 2.5 mm MAS probe head spinning at 25 kHz and all other measurements were carried out using a Bruker triple channel 4 mm MAS probe head spinning at rates between 8 and 10 kHz. ^{27}Al NMR spectra were recorded with a single pulse sequence with an 18 degree pulse duration of 1 μs and an interscan delay of 1 s. ^{19}F NMR spectra were taken using a rotor-synchronized Hahn-echo pulse sequence p1–τ1–p2–τ2–aq with a 90° pulse p1 = 5 μs and a 180° pulse p2 = 10 μs and an interscan delay of 5 s. Quantitative ^{29}Si NMR spectra were recorded using a high power proton decoupling direct excitation (DE) pulse sequence with a 45° pulse duration of 3 μs and an interscan delay of 180 s. ^{29}Si{^{1}H} CP MAS (CP = cross polarization) was performed with a ramped contact pulse of 3 ms and an interscan delay of 3 s. During the acquisition, ^{1}H heteronuclear decoupling was applied using the spinal-64 pulse scheme. ^{1}H and ^{29}Si NMR shifts were calibrated using tetramethylsilane (TMS). The saturated $Al(NO_3)_3$ solution was used for ^{27}Al NMR shift calibration. The ^{19}F NMR chemical shift was referenced to $CFCl_3$ using C_6F_6 (−164.9 ppm) as the external standard.

H_2 chemisorption. H_2 uptake measurements were used to titrate the surface metal atoms and to provide an estimate of the amount of active sites in reduced catalysts. Typically, 50 mg of the sample was loaded in a quartz reactor. Prior to dosing, the samples were reduced in flowing H_2 (1 h, 400 °C 3 °C min^{-1}), evacuated at 450 °C for 1 h to remove chemisorbed hydrogen and cooled to 80 °C under vacuum. Analysis was then performed at 80 °C by collecting an adsorption isotherm to determine the H_2 uptake.

2.5 Catalytic activity measurements

Before performing *n*-hexadecane hydroconversion activity tests, the Pd-loaded MOR catalysts were dried *in situ* at atmospheric pressure for 1 h in a He flow and 200 °C followed by a reduction in a H_2 flow at 60 bar. During reduction, the temperature was increased from 100 °C to 400 °C (a rate of 3 °C min^{-1}) followed by an isothermal period of 1 h. Subsequently, the catalyst layer was cooled down until 200 °C and the packed bed was saturated with an n-C_{16} liquid feed for 10 min (a flow rate of 1 ml min^{-1}). The reactor was operated at a H_2/n-C_{16} molar ratio of 20 and a weight hourly space velocity (WHSV) of 10 $g_{n\text{-}C_{16}}$ g_{cat}^{-1} h^{-1}. The reaction temperature was increased stepwise and the reaction was equilibrated for 3 h before product sampling. The reactor effluent was analyzed using a gas chromatograph equipped with an RTX-1 column and a flame ionization detector.

3. Results and discussion

3.1 Dealumination by hydrothermal NH_4F treatment

In order to optimize the NH_4F treatment, we varied the temperature, duration and NH_4F concentration of the as-synthesized ZSM-5 zeolite. Fig. 1a shows the influence of the temperature at a constant NH_4F concentration of 1 M and a treatment time of 6 h. The Si/Al ratio does not change significantly for treatment temperatures between 175 °C and 195 °C (Fig. 1a). Accordingly, we selected a temperature of 175 °C for further optimization. Fig. 1b shows that dealumination at 175 °C using a 1 M NH_4F solution leads to changes in the Si/Al ratio for the first 6 h. Notably, a small decrease of the Si/Al ratio was observed when the treatment was prolonged, which can be explained by a competition between dealumination and desilication as discussed in detail in the work of Qin *et al.*[30] Clearly, the rate of dealumination is substantially higher than the rate of desilication during the first 6 h in the slightly acidic 1 M NH_4F solution (pH ≈ 6 at 20 °C). In this approach, about 30% of the Al atoms can be removed from the zeolite framework. It is likely that, at a particular concentration of framework Al, desilication starts to compete with the dealumination process. This can be explained by an increase in the pH of the solution due to the slow release of NH_3, resulting from the dissociation of ammonium ions.

We also optimized the NH_4F concentration at a constant temperature of 175 °C and a reaction time of 6 h (Fig. 1c). Increasing the NH_4F concentration expectedly resulted in a higher degree of dealumination. Using a solution of 5 M NH_4F, about 90% of framework Al could be removed (Table 1). This degree of dealumination, however, had a negative effect on the crystallinity and the texture of the calcined zeolites. Table 1 and Fig. 2 demonstrate that, when the NH_4F concentration is raised above 1.5 M, the BET surface area and crystallinity of the zeolites are severely decreased due to the increased degree of desilication, provoked by enhanced dissociation of ammonium ions and/or higher concentration of *e.g.* HF and HF_2^- that can dissolve Si and Al at equal rates. Below this concentration, the zeolite crystals remain almost

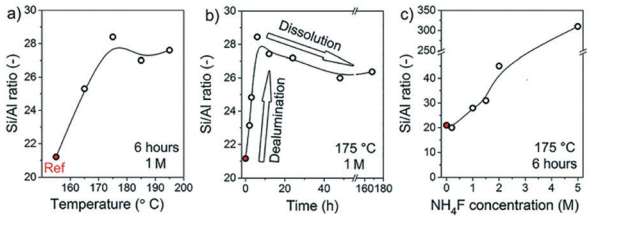

Fig. 1 Si/Al ratio of MFI crystals, derived from ICP, after NH_4F treatment: influence of (a) temperature after 6 h of treatment in 1 M NH_4F, (b) time at 175 °C in 1 M NH_4F and (c) NH_4F concentration at 175 °C and after 6 h of treatment.

Table 1 Composition and textural properties of TPA–MFI samples after the hydrothermal treatment with varying concentrations of NH_4F. Treatment conditions: 175 °C, 6 h

NH_4F treatment	Si/Al, ICP	FAl removed NMR, %	EFAl NMR, %	V_{micro}, $cm^3\ g^{-1}$ (*t*-plot method)	BET surface area, $m^2\ g^{-1}$	External surface area, $m^2\ g^{-1}$
Ref	21 ± 2	0	7.5	0.12	391	55
0.2 M	20 ± 2	7	8.5	0.12	370	55
1 M	28 ± 2	33	7.2	0.10	337	78
1.5 M	31 ± 2	41	8.7	0.10	318	46
2 M	45 ± 2	48	9.9	0.08	240	44
5 M	310 ± 10	87	~10	0.02	98	64

completely intact with retention of the textural properties of the reference sample (not treated with NH_4F).

Electron microscopy shows that the treatment of the MFI–TPA sample in a 1 M NH_4F solution did not lead to significant changes in crystal appearance (Fig. 3). No apparent defects in the treated crystals, such as mesopores, cracks or holes were observed upon careful examination of TEM and SEM images. As the morphology of the crystals remained unchanged, it is not likely that the sample has undergone a dissolution–recrystallization process in fluoride media, as reported earlier for template-free silicalite-1 zeolites.[31]

At this stage, we cannot exclude that partial recrystallization occurs at the near-surface layers. To study the surface region in more detail, we employed surface-sensitive XPS in combination with Ar sputtering.

The Si/Al ratio extracted from the XPS spectra are shown in Fig. 4. The Si/Al ratios of the parent MFI–TPA sample determined by both ICP and XPS are similar. The surface Si/Al ratio of the sample treated with NH_4F is significantly higher (~40%) than the value obtained after one minute of Ar etching. This finding points to preferential dealumination close to the surface, most likely caused by diffusion limitations experienced by the F^- ions. It should be noted that partial recrystallization of near surface layers might also explain this effect. The NH_4F dealumination procedure therefore creates a certain gradient of Al concentration within the crystals, as depicted by the inset in Fig. 4.

Further, we applied multinuclear NMR analysis to estimate structural changes after the treatment. An increase of the Q_3 signal at 100 ppm corresponding to $(SiO)_3Si–OH$ species in the ^{29}Si NMR spectra indicates that NH_4F treatment of MFI–TPA crystals results in a small amount of silanol groups. This signal is visible as a shoulder in the direct excitation spectrum and as a cross peak in the ^1H-^{29}Si CP spectrum (Fig. 5a and b).

It is not possible to quantify these new silanol groups, as the Q_3 and Q_4 (1Al) signals could not be resolved. However,

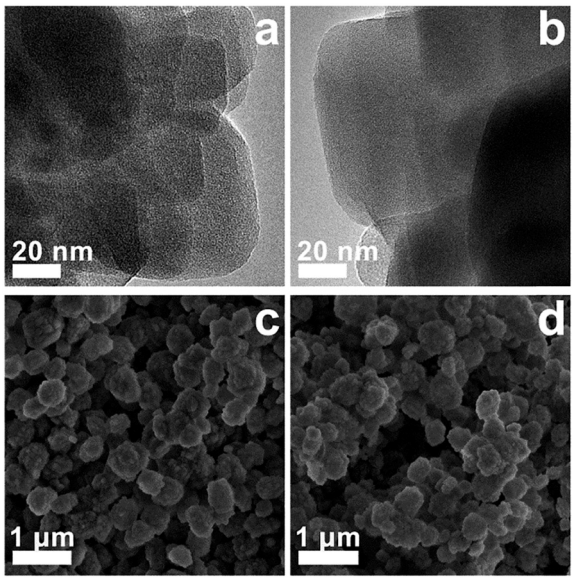

Fig. 3 TEM (a and b) and SEM (c and d) images of MFI–TPA samples before (a and c) and after (b and d) NH_4F treatment. Treatment conditions: 175 °C, 6 h, 1 M NH_4F.

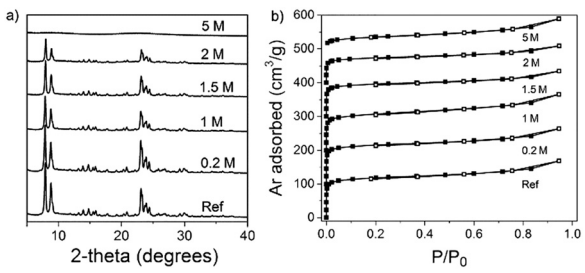

Fig. 2 XRD patterns (a) and Ar physisorption isotherms (b) of calcined MFI–TPA samples treated in NH_4F solution of varying concentrations. The isotherms are offset for clarity by 100 $cm^3\ g^{-1}$. (closed symbols – adsorption branch, open symbols – desorption branch. Treatment conditions: 175 °C, 6 h).

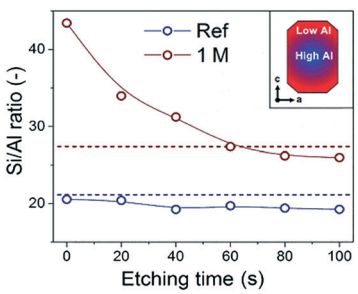

Fig. 4 Si/Al ratios derived from XPS for MFI samples before (blue) and after (red) NH_4F treatment. Dashed lines represent Si/Al ratios from ICP. The inset illustrates gradient of Al concentration within the zeolite crystals. Treatment conditions: 175 °C, 6 h, 1 M NH_4F.

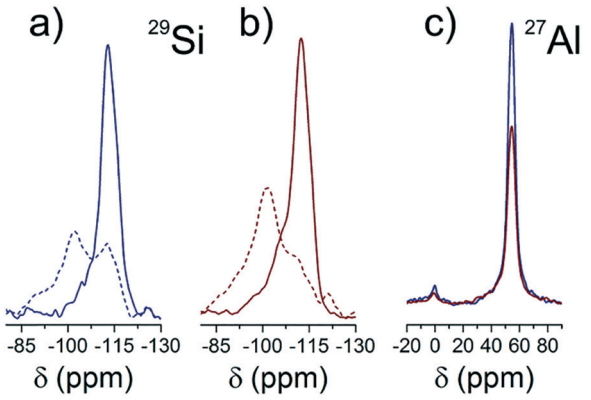

Fig. 5 Weight-normalized ^{29}Si NMR spectra of (a) reference MFI and (b) after NH_4F treatment. Solid lines – direct excitation experiments, dashed lines – ^{1}H-^{29}Si cross polarization experiments. (c) ^{27}Al NMR spectra of reference MFI (red) and after NH_4F treatment (blue). Treatment conditions: 175 °C, 6 h, 1 M NH_4F.

we expect the number of such silanol defects to remain low, because the crystallinity and microporosity of the samples were high after optimized NH_4F treatment. Overall, the formation of silanol groups suggests that the presence of aluminum in the framework influences the exchange of SiO^- species with F^-, as also shown by Tuel and co-workers for NH_4F treatment of as-synthesized pure-silica zeolites.[21] The absence of fluoride signals in the ^{19}F NMR spectrum of NH_4F-treated and calcined ZSM-5 crystals (Fig. S2†) evidences that during washing all weakly soluble AlF_3, $NH_4[AlF_4]$ and $(NH_4)_3[AlF_6]$ compounds were removed.

The treatment did not lead to additional extraframework Al species (EFAl) during NH_4F treatment as can be derived from the ^{27}Al NMR spectra (Fig. 5c). The main difference effected by the treatment is a decrease in the framework Al signal at 55 ppm. These results suggest that aluminum is mostly extracted from tetrahedral positions in the MFI framework rather than from octahedral positions.

Analysis of the OH stretching vibration bands in the 3400–3800 cm^{-1} region of the IR spectra (Fig. 6) confirms the above findings. A slight increase of the band at 3745 cm^{-1}, accompanied by a small broadening of this signal, points at a larger amount of terminal silanol groups and a nearly negligible amount of silanol nests.[32] The band at 3660 cm^{-1}, corresponding to extraframework Al–OH groups, is only slightly affected by the treatment, while the concentration of bridging OH expectedly decreased due to the NH_4F treatment.

3.2 Influence of the template stabilization

Neither Ar physisorption (Fig. 2b) nor electron microscopy (Fig. 3) indicated that the dealuminated zeolites contain mesopores. This is the main difference between the treatment of template-free and template-stabilized zeolite crystals. Valtchev and co-workers reported that NH_4F treatment of template-free ZSM-5 resulted in the non-selective extraction of Si and Al and formation of mesopores revealing a mosaic

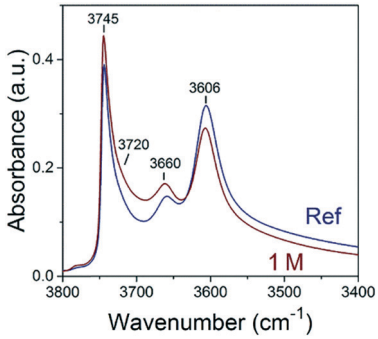

Fig. 6 Weight-normalized IR spectra of the dehydrated reference and NH_4F-treated ZSM-5 samples. Treatment conditions: 175 °C, 6 h, 1 M NH_4F.

structure of initially aggregated crystals.[30] The presence of template molecules before and after the treatment inside the pores of MFI, as shown by the thermogravimetric analysis (TGA) in Fig. 7, results in strong stabilization of the zeolite framework and allows selective removal of Al atoms without formation of additional non-zeolitic pores.

To further explore the stabilizing role of TPA cations, we performed several additional experiments. First, we calcined a parent MFI sample to remove TPA^+ from the pores. Second, we prepared MFI crystals by replacing TPAOH in the synthesis gel with pentaerythritol (PET), an uncharged tetraol, which is geometrically similar to TPAOH and can act as an SDA for MFI growth (Fig. 8a).[33] Both samples were treated under the earlier optimized conditions. The NH_4F treatment of the template-free MFI sample led to a severe degradation of the crystalline microporous structure (Fig. 8b and S3,† Table 2) and formation of visible defects, imperfections and even amorphous domains (Fig. 9). Yet, when the MFI-PET sample was treated about 40% of the Al atoms were removed (Fig. 8c and S4†) without significant structural degradation (Table 2). These results point to the pivotal role of the template in stabilizing the zeolite during NH_4F dealumination. Indeed, the presence of PET molecules and especially charged TPA^+ cations inside the MFI pores makes it possible

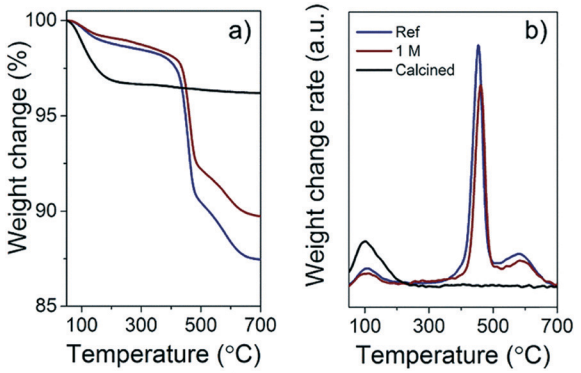

Fig. 7 TGA (a) and DTG (b) profiles of MFI samples before (blue) and after (red) NH_4F treatment and the pre-calcined (black) sample. Treatment conditions: 175 °C, 6 h, 1 M NH_4F.

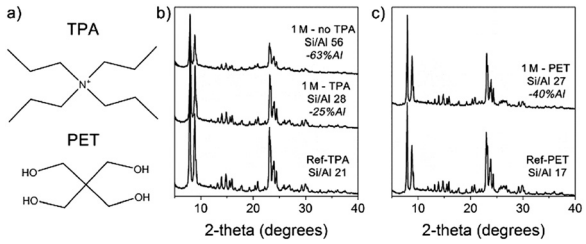

Fig. 8 (a) Tetrapropylammonium (TPA^+) and pentaerythritol (PET) SDAs applied for the synthesis of MFI zeolites. XRD patterns and Si/Al ratios of TPA (b) and PET (c) MFI zeolites before and after NH_4F treatment. Treatment conditions: 175 °C, 6 h, 1 M NH_4F.

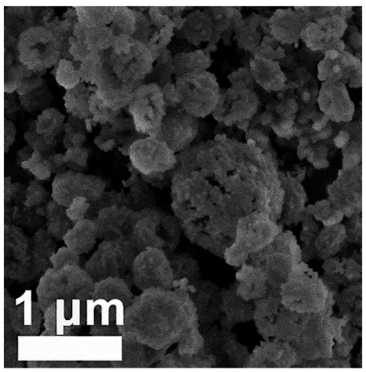

Fig. 9 SEM image of TPA-free MFI crystals after calcination in air and NH_4F treatment. Treatment conditions: 175 °C, 6 h, 1 M NH_4F.

to remove a significant fraction of Al atoms, while keeping the framework essentially intact.

To summarize, mild dealumination with an aqueous NH_4F solution of the as-synthesized ZSM-5 zeolite constitutes a promising method for the synthesis of high-silica zeolite materials, particularly for topologies that are difficult to prepare in the high-silica form directly. As high-silica zeolites are (hydro)thermally more stable and often preferred for catalytic and adsorptive applications[34,35] and membrane separations,[36] the developed NH_4F dealumination of template-stabilized zeolite materials is a valuable addition to the existing synthetic repertoire.

3.3 Optimization NH_4F treatment for the MOR zeolite

Compared to ZSM-5 zeolite which can be synthesized in a wide compositional range,[37,38] mordenite (MOR) zeolite crystallizes typically at a Si/Al ratio below 10.[39] The preferred ratio for catalytic applications is however usually higher than 10.[40] Accordingly, post-treatment dealumination of bulk MOR zeolite *via* steaming and leaching of bulk MOR zeolite is widely employed to reach the desired acidic properties.[41] These approaches usually also lead to formation of beneficial mesoporosity. Here, we employed our method of NH_4F treatment to tune the Si/Al ratio of MOR zeolite. The starting material is a MOR zeolite prepared with a charged C_{16}NMP (*N*-cetyl-*N*-methylpyrrolidinium cation) as the SDA.[42] The use of this amphiphilic SDA results in a hierarchical pore structure with potential benefits to catalysis. We demonstrated that, after loading of Pd nanoparticles, this zeolite shows improved performance in bifunctional *n*-hexadecane hydroconversion compared to bulk MOR zeolite because of a reduced amount of acid sites in the main 12-membered ring channels as well as the presence of mesopores. A drawback of this material is that the concentration of Brønsted acid sites (BAS) is too high for hydroisomerization, resulting in a high extent of secondary cracking. We stress here that MOR zeolite is usually prepared using Na^+ as the inorganic SDA. The synthesis without an organic void-filling SDA means that we cannot treat a bulk reference with NH_4F as a reference.

A conventional MOR sample denoted as MOR-H (hierarchical) was synthesized according to the procedure described in our previous report.[42] The sample constituted a highly crystalline MOR zeolite with a Si/Al ratio of 9 (Fig. 10). The duration and NH_4F concentration were optimized for the mild dealumination treatment. An increase in the Si/Al ratio from 9.0 to 10.7 was observed after 2 h treatment using a 1 M NH_4F solution (Fig. 10a). The fact that the Si/Al ratio remains similar during prolonged treatment might be due to competing desilication. Extensive dealumination up to 40% was observed with an increase of the NH_4F concentration

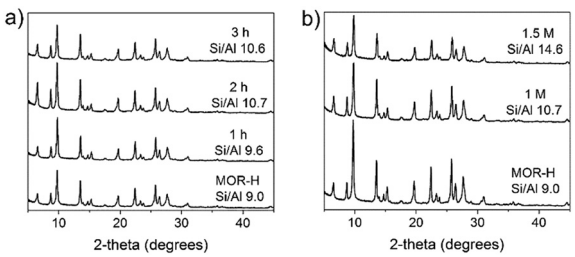

Fig. 10 Optimization of the treatment of the MOR-H zeolite with NH_4F. XRD patterns and Si/Al ratios of the MOR-H zeolite before and after NH_4F treatment at different (a) times and (b) NH_4F concentrations at 175 °C.

Table 2 Physico-chemical properties of the zeolites upon NH_4F hydrothermal treatment with different stabilization cations. Treatment conditions: 175 °C, 6 h, 1 M NH_4F

The sample	Si/Al, ICP	V_{micro}, $cm^3\ g^{-1}$ (*t*-plot method)	BET surface area, $m^2\ g^{-1}$	External surface area, $m^2\ g^{-1}$
Ref – TPA	21 ± 2	0.12	391	55
1 M – TPA	28 ± 2	0.10	337	78
1 M – no TPA	56 ± 2	0.04	159	33
Ref – PET	17 ± 2	0.10	304	21
1 M – PET	27 ± 2	0.08	283	37

from 1 M to 1.5 M (Fig. 10b, Table S1†). The ^{27}Al NMR spectra showed a decrease in the signal at 55 ppm due to framework Al (Fig. S5a†). This finding is supported by the IR spectra (Fig. S5b†), where it is seen that the band at 3605 cm^{-1} attributed to bridging acidic hydroxyl groups decreases significantly due to the NH_4F treatment.

Electron microscopy shows that the conventional MOR-H sample is composed of stacked nanorods with a width of about 50 nm, resulting in agglomerates with a size of ~10 μm (Fig. 11a and d). In comparison to ZSM-5, dealumination of MOR results in more significant textural changes such as an increase of the external surface area, the mesoporous volume (Fig. S5c and Table S1†) and partly alterations to the morphology of the zeolite with formation of some amorphous debris at the short edges of the crystals (Fig. 11b, c, e and f).

This might be due to the higher accessibility for F^- ions of MOR-H nanorods stabilized by C_{16}NMP. Deeper dealumination and desilication can also explain the formation of a secondary amorphous spherical aluminosilicate phase at increased NH_4F concentration (1.5 M, Fig. S6†). As we only observe a slight increase of extraframework Al (Table S1†), we infer that the formed amorphous phase mainly consists of silica with a low Al content. Accordingly, we assume that the acidity of this amorphous phase should be low compared to the zeolite part. Judging from the XRD pattern (Fig. 10), the amount of this amorphous silica phase is small. However, its presence in the final product leads to some changes in the textural properties *e.g.* an increase in BET and external surface areas while microporous MFI samples behaved differently (Tables 1 and S1†). Based on the TEM image (Fig. S6†) and the isotherm shape (Fig. S5c†), this sidephase is most likely a mesoporous silica with a high surface area. Additionally, the increased degree of dealumination leading to a small increase in the number of EFAl explains the higher concentration of Lewis acid sites (LAS) (Table S2†). We also found that NH_4F treatment of a calcined MOR-H sample led to complete destruction of the crystalline MOR structure (Fig. S7†), emphasizing the key role of the organic template during mild dealumination with NH_4F.

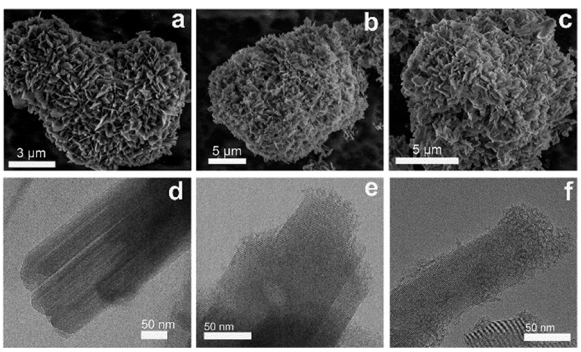

Fig. 11 SEM (a–c) and TEM (d–f) images of MOR samples before (a and d) and after treatment with (b and e) 1 M and (c and f) 1.5 M NH_4F solution. Treatment conditions: 175 °C, 2 h.

3.4 Catalytic performance in *n*-hexadecane hydroconversion

The catalytic performance in *n*-paraffin hydroconversion was determined for MOR-H before and after treatment in NH_4F solution with concentrations of 1 M and 1.5 M. The conventional and treated MOR zeolites were loaded with 1 wt% Pd, calcined at 450 °C in flowing air for 4 h and reduced prior to reaction. The conversion of *n*-hexadecane as a function of temperature is shown in Fig. 12a. The ratio between metallic Pd and BAS (Pd/H^+ atomic ratio) varied between 0.16 and 0.25 (Table S2†), indicating that there is a suitable balance between metal and acid sites in these catalysts.[43,44]

We first compare MOR-H with the sample obtained after 1 M NH_4F treatment in *n*-hexadecane hydroconversion. Both samples exhibit nearly similar apparent activation energies of 146 kJ mol^{-1} and 139 kJ mol^{-1}, respectively (Fig. 12b). Thus, the lower conversion observed for the NH_4F-treated sample is mainly due to the lower amount of BAS.

Fig. 13 shows the product distribution as a function of the temperature for these samples. Conventional MOR-H presents a high selectivity to isomers, especially multi-branched isomers, at low conversion (<20%). At higher conversion, the selectivity to cracked products increases. The MOR-H sample treated with a 1 M NH_4F solution exhibits a similar product

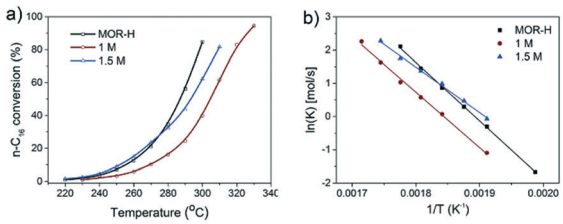

Fig. 12 Conversion of *n*-hexadecane as a function of the reaction temperature (a) and Arrhenius plot (b).

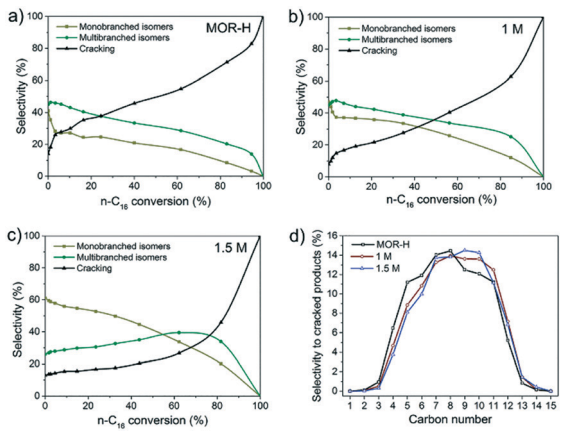

Fig. 13 Total product selectivity as a function of *n*-hexadecane conversion for MOR-H (a), 1 M (b) and 1.5 M (c) catalysts. Selectivity to cracked products obtained at *ca.* 50% *n*-hexadecane conversion (d). Experimental conditions: WHSV = 10 h^{-1}, H_2/n-C_{16} molar ratio = 20, *P* = 60 bar, 1 wt% Pd.

distribution, although the high isomer selectivity is maintained in a wider conversion range (up to 40%) consistent with the lower acidity. The MOR-H sample treated with 1.5 M NH_4F behaves substantially differently as a catalyst. The apparent activation energy of this catalyst is significantly lower (114 kJ mol^{-1}). Despite having the lowest acidity, the conversion of *n*-hexadecane is nearly similar to that of the MOR-H sample at temperatures below 280 °C. As it is well-known that the rate of *n*-paraffin hydroconversion for tubular MOR zeolite is limited by mass transport limitations, we speculate that the increased activity of this sample is due to higher accessibility of the MOR micropores provoked by changes in the morphology of the MOR nanorods after the treatment.

This sample also exhibits a higher selectivity to monobranched isomers at low conversion, while a high multibranched isomer selectivity is maintained up to a conversion of 60%. These selectivity differences in isomerization products between the three MOR zeolites likely originate from variations in diffusion rates. While the distribution of cracked paraffins for MOR-H shifted slightly to lighter paraffins (Fig. 13d) indicative of a contribution of secondary cracking, the two NH_4F-samples showed a more symmetric distribution of cracked products, closely resembling the distribution expected for the ideal hydrocracking regime.[45] This can be attributed to the lower acidity of these materials. The used Pd/MOR catalysts showed similar activity to the fresh ones and were able to reach 40% conversion at the same temperature according to the activation plot (Fig. 12).

4. Conclusions

In this work we described a method to dealuminate high-silica zeolites by a hydrothermal treatment with an aqueous solution of NH_4F. Under optimized conditions, it is possible to remove 30–50% of Al atoms from the ZSM-5 zeolite framework and significantly more than 50% of Al from the crystal surface without structural degradation or formation of extraframework Al species. Template stabilization with an organic template such as tetrapropylammonium or pentaerythritol is essential to avoid complete degradation of the zeolite crystals. We applied this dealumination approach to MOR zeolite, which cannot be prepared at a high Si/Al ratio. As an example, we dealuminated hierarchical MOR zeolite prepared with the SDA C_{16}NMP, which also acts as a mesoporogen. Optimizing the NH_4F treatment led to an increase in the Si/Al ratio from 9 to nearly 15 and the generation of more favourable textural properties. When loaded with Pd, this zeolite performed substantially better in the bifunctional *n*-hexadecane hydroconversion than the reference mesoporous MOR sample. The higher accessibility of BAS for the reactant led to a higher activity despite the lower acidity. The improved balance between acid sites and metal hydrogenation sites also suppressed secondary cracking, yielding a nearly ideal hydrocracking pattern for the optimized sample.

Conflicts of interest

There are no conflicts to declare.

Acknowledgements

The authors thank the Impuls program of the Eindhoven University of Technology for financial support. Emiel J. M. Hensen also acknowledges financial support from a TOP grant of the Netherlands Organisation for Scientific Research.

Notes and references

1 C. S. Cundy and P. A. Cox, *Chem. Rev.*, 2003, **103**, 663–701.
2 E. M. Flanigen and R. L. Patton, *U.S. Pat.*, 4073865, 1978.
3 R. E. Morris, A. Burton, L. M. Bull and S. I. Zones, *Chem. Mater.*, 2004, **16**, 2844–2851.
4 M. Dodin, J. L. Paillaud, Y. Lorgouilloux, P. Caullet, E. Elkaïm and N. Bats, *J. Am. Chem. Soc.*, 2010, **132**, 10221–10223.
5 M. A. Camblor, L. A. Villaescusa and M. J. Díaz Cabañas, *Top. Catal.*, 1999, **9**, 59–76.
6 T. Moteki and R. F. Lobo, *Chem. Mater.*, 2016, **28**, 638–649.
7 S. Valencia, A. Martínez, P. Esteve, M. A. Camblor, J. M. Guil, T. Blasco, A. Corma and J. A. Perdigón-Melón, *J. Phys. Chem. B*, 1998, **102**, 75–88.
8 A. Rojas, M. L. San-Roman, C. M. Zicovich-Wilson and M. A. Camblor, *Chem. Mater.*, 2013, **25**, 729–738.
9 P. Caullet, J. L. Paillaud, A. Simon-Masseron, M. Soulard and J. Patarin, *C. R. Chim.*, 2005, **8**, 245–266.
10 K. Zhang, R. P. Lively, J. D. Noel, M. E. Dose, B. A. McCool, R. R. Chance and W. J. Koros, *Langmuir*, 2012, **28**, 8664–8673.
11 S. Prodinger, H. Shi, S. Eckstein, J. Z. Hu, M. V. Olarte, D. M. Camaioni, M. A. Derewinski and J. A. Lercher, *Chem. Mater.*, 2017, **29**, 7255–7262.
12 L. Tosheva, Z. Qin, V. Valtchev, L. Lakiss, J.-P. Gilson, A. Vicente and C. Fernandez, *Adv. Funct. Mater.*, 2013, **24**, 257–264.
13 X. Zhu, N. Kosinov, J. P. Hofmann, B. Mezari, Q. Qian, R. Rohling, B. M. Weckhuysen, J. Ruiz-Martínez and E. J. M. Hensen, *Chem. Commun.*, 2016, **52**, 3227–3230.
14 X. Zhu, N. Kosinov, A. V. Kubarev, A. Bolshakov, B. Mezari, I. Valastyan, J. P. Hofmann, M. B. J. Roeffaers, E. Sarkadi-Pribóczki and E. J. M. Hensen, *ChemCatChem*, 2017, **9**, 3470–3477.
15 M. Li, Y. Zhou, C. Ju and Y. Fang, *Appl. Catal., A*, 2016, **512**, 1–8.
16 X. Chen, A. Vicente, Z. Qin, V. Ruaux, J. P. Gilson and V. Valtchev, *Chem. Commun.*, 2016, **52**, 3512–3515.
17 S. Du, X. Chen, Q. Sun, N. Wang, M. Jia, V. Valtchev and J. Yu, *Chem. Commun.*, 2016, **52**, 3580–3583.
18 Z. Qin, J. P. Gilson and V. Valtchev, *Curr. Opin. Chem. Eng.*, 2015, **8**, 1–6.
19 Y. Kuwahara, T. Kamegawa, K. Mori and H. Yamashita, *Chem. Commun.*, 2008, 4783–4785.

20 N. Kosinov, V. G. P. Sripathi and E. J. M. Hensen, *Microporous Mesoporous Mater.*, 2014, **194**, 24–30.
21 X. Liu, U. Ravon and A. Tuel, *Angew. Chem., Int. Ed.*, 2011, **50**, 5900–5903.
22 A. Burton, *Catal. Rev.: Sci. Eng.*, 2017, **60**, 1–44.
23 S. Mintova, V. Valtchev, T. Onfroy, C. Marichal, H. Knözinger and T. Bein, *Microporous Mesoporous Mater.*, 2006, **90**, 237–245.
24 G. Cruciani, *J. Phys. Chem. Solids*, 2006, **67**, 1973–1994.
25 M. C. Silaghi, C. Chizallet and P. Raybaud, *Microporous Mesoporous Mater.*, 2014, **191**, 82–96.
26 L. H. Ong, M. Dömök, R. Olindo, A. C. Van Veen and J. A. Lercher, *Microporous Mesoporous Mater.*, 2012, **164**, 9–20.
27 L. D. Borges and J. L. de Macedo, *Microporous Mesoporous Mater.*, 2016, **236**, 85–93.
28 Y. Wang, R. Otomo, T. Tatsumi and T. Yokoi, *Microporous Mesoporous Mater.*, 2016, **220**, 275–281.
29 Y. Zhang, H. Wang and R. Chen, *RSC Adv.*, 2015, **5**, 67841–67848.
30 Z. Qin, J.-P. Gilson, O. Ersen, K. Bozhilov, S. Mintova, P. Boullay, M. Jaber, G. Melinte and V. Valtchev, *Angew. Chem., Int. Ed.*, 2016, **55**, 15049–15052.
31 L. Burel and A. Tuel, *Microporous Mesoporous Mater.*, 2013, **174**, 90–99.
32 S. Bordiga, C. Lamberti, F. Bonino, A. Travert and F. Thibault-Starzyk, *Chem. Soc. Rev.*, 2015, **44**, 7262–7341.
33 T. Biligetu, Y. Wang, T. Yokoi, T. Tatsumi and H. Mochizuki, *Chem. Lett.*, 2017, **46**, 798–800.
34 H. Song, H. Gao, H. Song, G. Yang and X. Li, *Ind. Eng. Chem. Res.*, 2016, **55**, 3813–3822.
35 J. Wu, H. Zhu, Z. Wu, Z. Qin, L. Yan, B. Du, W. Fan and J. Wang, *Green Chem.*, 2015, **17**, 2353–2357.
36 N. Kosinov, C. Auffret, G. J. Borghuis, V. G. P. Sripathi and E. J. M. Hensen, *J. Membr. Sci.*, 2015, **484**, 140–145.
37 A. P. Jacobs and J. A. Martens, *Studies in Surface Science and Catalysis*, 1987, vol. 33, pp. 47–111.
38 L. Shirazi, E. Jamshidi and M. R. Ghasemi, *Cryst. Res. Technol.*, 2008, **43**, 1300–1306.
39 A. A. Shaikh, P. N. Joshi, N. E. Jacob and V. P. Shiralkar, *Zeolites*, 1993, **13**, 511–517.
40 P. K. Bajpal, M. S. Rao and K. V. G. K. Gokhale, *Ind. Eng. Chem. Prod. Res. Dev.*, 1978, **17**, 223–227.
41 K. Chung, *Microporous Mesoporous Mater.*, 2008, **111**, 544–550.
42 A. Bolshakov, D. Romero, A. Van Hoof, N. Kosinov and E. Hensen, *ChemCatChem*, 2019, **11**, 2803–2811.
43 N. Batalha, L. Pinard, C. Bouchy, E. Guillon and M. Guisnet, *J. Catal.*, 2013, **307**, 122–131.
44 M. J. Ramos, A. de Lucas, J. L. Valverde, P. Sánchez and F. Dorado, *Appl. Catal., A*, 2005, **294**, 215–225.
45 E. U. Schlunder, P. Krotzsch and W. Hennecke, *Chem. Ing. Tech.*, 1970, **42**, 333–428.